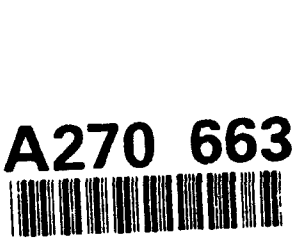

ARMY RESEARCH LABORATORY

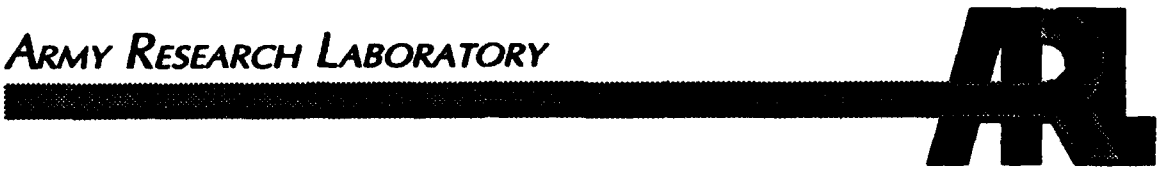

Blade and Hub Loads of Ballistically Damaged Helicopter Rotors

Ki C. Kim

ARL-TR-235 October 1993

NOTICES

Destroy this report when it is no longer needed. DO NOT return it to the originator.

Additional copies of this report may be obtained from the National Technical Information Service, U.S. Department of Commerce, 5285 Port Royal Road, Springfield, VA 22161.

The findings of this report are not to be construed as an official Department of the Army position, unless so designated by other authorized documents.

The use of trade names or manufacturers' names in this report does not constitute indorsement of any commercial product.

REPORT DOCUMENTATION PAGE

Form Approved
OMB No. 0704-0188

1. AGENCY USE ONLY (Leave blank)	2. REPORT DATE	3. REPORT TYPE AND DATES COVERED
	October 1993	Final, April 1992 - May 1993

4. TITLE AND SUBTITLE
Blade and Hub Loads of Ballistically Damaged Helicopter Rotors

5. FUNDING NUMBERS
PR: 1L162618AH80

6. AUTHOR(S)
Ki C. Kim

7. PERFORMING ORGANIZATION NAME(S) AND ADDRESS(ES)
U.S. Army Research Laboratory
ATTN: AMSRL-SL-BA
Aberdeen Proving Ground, MD 21005-5068

8. PERFORMING ORGANIZATION REPORT NUMBER

9. SPONSORING / MONITORING AGENCY NAME(S) AND ADDRESS(ES)
U.S. Army Research Laboratory
ATTN: AMSRL-OP-CI-B (Tech Lib)
Aberdeen Proving Ground, MD 21005-5066

10. SPONSORING / MONITORING AGENCY REPORT NUMBER
ARL-TR-235

11. SUPPLEMENTARY NOTES

12a. DISTRIBUTION / AVAILABILITY STATEMENT
Approved for public release; distribution is unlimited.

12b. DISTRIBUTION CODE

13. ABSTRACT *(Maximum 200 words)*

The effects of (simulated) ballistic damage on helicopter rotor blade response and rotor hub loads are investigated. A finite element formulation based on Hamilton's principle is used for structural analysis, and aerodynamic loads are calculated using quasisteady aerodynamic theory. Each blade is treated as being composed of elastic beams undergoing flap bending, lag bending, elastic twist, and axial deflections. Dynamic responses of multi-blade rotor systems are calculated from nonlinear periodic normal mode equations using a finite element in time scheme.

Results are calculated for the SA349/2 Gazelle helicopter for both undamaged and damaged blade configurations. Blade damage effects are determined in terms of blade mode shapes and frequencies, aeroelastic response, and rotor hub loads. Blade dissimilarity due to ballistic damage can induce a large 1/rev vibratory component on the rotor hub.

14. SUBJECT TERMS
helicopters; rotor blades; hub loads; aerodynamics; helicopter aeroelasticity; coupled trim solution

15. NUMBER OF PAGES
38

16. PRICE CODE

17. SECURITY CLASSIFICATION OF REPORT	18. SECURITY CLASSIFICATION OF THIS PAGE	19. SECURITY CLASSIFICATION OF ABSTRACT	20. LIMITATION OF ABSTRACT
UNCLASSIFIED	UNCLASSIFIED	UNCLASSIFIED	SAR

INTENTIONALLY LEFT BLANK.

Table of Contents

INTENTIONALLY LEFT BLANK.

List of Figures

INTENTIONALLY LEFT BLANK.

List of Tables

INTENTIONALLY LEFT BLANK.

Acknowledgment

The author would like to to express gratitude to Mr. Stephen F. Polyak, a team leader of Engineering Analysis Team (EAT) in the Air Systems Branch (ASB) of the US Army Research Laboratory (ARL), for his invaluable support during the course of this research. The author would also like to thank Dr. James N. Walbert, a chief of Air Systems Branch (ASB) of ARL, for his support.

INTENTIONALLY LEFT BLANK.

Nomenclature

c	Blade chord.
c_0	Lift coefficient at zero angle of attack.
c_1	Lift curve slope.
C_d	Blade section drag coefficient.
C_l	Blade section lift coefficient.
$C_{m_{ac}}$	Blade section pitching moment coefficient about aerodynamic center.
C_{D_f}	Fuselage drag coefficient.
C_{l_f}	Fuselage rolling moment coefficient.
C_{L_f}	Fuselage lift coefficient.
C_{m_f}	Fuselage pitching moment coefficient.
C_{n_f}	Fuselage yawing moment coefficient.
C_Q	Rotor-shaft torque coefficient.
C_w	Helicopter weight coefficient.
d_0	Viscous drag coefficient.
d_1, d_2	Pressure drag coefficients.
D_F	Fuselage drag.
EI_y	Flap-wise bending stiffness.
EI_z	Chord-wise bending stiffness.
f_0, f_1	Pitching moment coefficients.
GJ	Effective sectional torsional stiffness.
$\bar{h}$	Vertical distance from helicopter c.g. to hub center.
l_i	Length of the ith beam element.

m	Blade section mass.
M	Mach number.
M_{inc}	Incident Mach number normal to chord.
m_o	Reference blade section mass.
N_b	Blade number.
$\mathbf{q}$	Global displacement vector.
R	Blade radius.
T	Rotor thrust.
u	Blade displacement in the axial direction.
v	Blade displacement in the lead-lag direction.
V	Helicopter forward speed.
w	Blade displacement in the flap-wise direction.
x_{cg}, y_{cg}	Hub center position relative to helicopter c.g. in the X and Y directions, respectively.
X_t	Distance between main rotor hub and tail rotor hub.
Y_F	Fuselage side force.
Y_{tr}	Tail rotor thrust.
α	Blade section angle of attack.
α_{HP}	Hub plane tilt angle relative to flight direction.
α_s	Longitudinal shaft tilt relative to wind axis.
β_0	Rotor coning angle.
β_{1s}, β_{1c}	Lateral and longitudinal disk tilt angle, respectively.
$\beta_l, \beta_d, \beta_m$	Aerodynamic deficiency functions because of blade damage.

θ_{1c}, θ_{1s}	Lateral and longitudinal cyclic trim inputs, respectively.
$\theta_{.75}$	Collective blade pitch at 0.75% radius.
θ_{FP}	Helicopter flight path angle relative to the longitudinal axis.
μ	Advance ratio.
σ	Rotor solidity ratio.
$\hat{\phi}$	Blade twist.
ϕ_s	Lateral shaft tilt.
Ω	Rotor rotational speed.

INTENTIONALLY LEFT BLANK.

I. Introduction

1. Background

Helicopters are frontline systems in most of the world's armed forces, with combat missions including troop insertion, observation and attack. Operational tactics typically employ low level flight to mask the helicopter's presence. Although this can conceal the aircraft from long range threats, the aircraft may still be exposed to attack from nearby small arms and light anti-aircraft artillery (e.g., 23 and 30 mm). Combat experience shows that rotor blades, particularly those of the main rotor, are often hit. While the rigorous application of damage-tolerant materials and vulnerability reduction design principles yields high levels of survivability, ballistic damage to the blade(s) (particularly from high-explosive projectiles) may still affect the performance capabilities and airworthiness of the vehicle.

Vibrations generated by the damaged rotor system may be severe enough to compromise the structural integrity of rotor/hub subsystem, to cause the crew to abort the mission, or force the aircraft to land. Damage to the rotor subsystem may also induce an aeroelastic instability that can cause loss of flight control and an attrition kill. Currently, with respect to vulnerability assessment, there is insufficient understanding of rotor blade ballistic damage effects on the aeroelastic response/stability of the rotor system and the associated helicopter performance and vibratory loads. An understanding of these effects is not only essential to accurately assess the level of vulnerability but also benefits helicopter survivability improvement efforts.

Most previous ballistic vulnerability studies involving helicopter rotors were simply conducted on isolated blades, which were statically evaluated, sometimes with axial loading. Using this approach, one can locally identify the effects of damage on the blade structural properties, such as the changes in local strength and strain or residual stress. Those studies, however, may not be directly applied to assessing the performance of a whole helicopter (i.e., with rotor-fuselage coupling) suffering blade damage in flight. In the present study, a specialized aeroelastic analysis has been performed to investigate helicopter response to in-flight main rotor blade damage.

In the context of the Army Research Laboratory's (ARL) Process Structure for analyzing combat system (e.g., helicopter) vulnerability, this research, and its associated engineering based methods, addresses the mapping from Level 2, the Target Component Damage State to Level 3, the Target Capability State (i.e, $O_{2,3}$ mapping); other levels include 1, Threat/Target Initial Conditions and 4, Target Combat Utility. A significant feature of this process is that at each level (or space) distinct, measurable information is available defining the threat/target encounter and vulnerability/lethality outcome. For example, here physical and aerodynamic factors defining rotor blade damage (Level 2) are mapped via engineering methods into parameters which define the rotor and helicopter system's functional capability (Level 3); all the defining terms are explicit and measurable through experimen-

tation. Note also that ambient (e.g, air density) and operating factors (e.g., forward flight velocity) (defined at Level 1) are accounted for in the methodology and provide realistic variable scenario capability. Application of these and other engineering analysis tools to the Vulnerability/Lethality Process Structure will occur largely through implementation in the Degraded States Vulnerability Methodology for level $O_{2,3}$ mapping now under development for aircraft targets at ARL.

2. Present Study

The objective of the current research is to investigate the effects of (simulated) ballistic damage on helicopter rotor blade response and hub loads.

This investigation was performed using the UMARC helicopter aeroelastic analysis computer code [1]. A finite element procedure is used for a structural analysis of damaged rotor blades, and rotor aerodynamic loads are calculated using quasisteady aerodynamic theory. Dynamic responses of helicopter rotor subsystems are calculated from periodic normal mode equations using a finite element method in time. Also, in the present study, results of wind tunnel tests of the damaged rotor blades [2] are used to include the aerodynamic performance degradation of a ballistically damaged blade.

Results are first calculated for the SA349/2 Gazelle, an advanced geometry three-bladed articulated rotor helicopter, with undamaged blade configuration. Results then are calculated for this helicopter with simulated blade damage configurations. The effects of this damage on helicopter response and loads are determined in terms of blade flap-lag-torsion frequency and modal shapes, blade aeroelastic response, and hub load variations.

The present study includes several new features that have not been previously addressed in the literature.

1. Consistent helicopter rotor blade damage modeling, including aerodynamic and structural interactions, is incorporated in the aeroelastic analysis.

2. Aerodynamic properties of damaged blade estimated from the results of wind tunnel tests with actual helicopter hardware.

3. The ultimate issues of aircraft flyability and controllability for given damages are discussed in the context of aircraft vulnerability assessment.

II. Formulation

The baseline helicopter aeroelastic code used in this investigation is a comprehensive aeroelastic analysis based on finite element theory in space and time [1].

The rotor blade is assumed to be an elastic beam undergoing flap bending, lag bending, elastic twist, and axial deflections. The helicopter fuselage is assumed to be a rigid body undergoing six degrees-of-freedom movement. Each blade is discretized into a number of beam elements, and for each element, there is a continuity of displacement and slope for flap (w) and lag (v) deflections and a continuity of displacement for axial (u) and torsion ($\hat{\phi}$) deflections. There are two internal nodes for axial displacement and one for elastic twist resulting in a total of 15 degrees of freedom for each element (see Figure 1). The formulation for the blade and fuselage equations of motion is based on Hamilton's principle. The analysis is developed for helicopters with nonuniform rotor blades having pretwist, precone, and chord-wise offsets of the center of mass, aerodynamic center and tension center from the elastic axis.

Aerodynamic loads are calculated using quasisteady strip theory. Noncirculatory aerodynamic forces are also included. To include the effect of high angle of attack flows, a dynamic stall model proposed by Johnson [3] is incorporated. Dynamic stall characterizes the delay in flow separation because of unsteady angle of attack, and the shedding of a vortex from the leading edge of the airfoil when it gets into a deep stall condition. These effects are introduced in the calculation of section lift, drag and pitching moment. For this, the time history of blade motion of the previous cycle is used.

Aerodynamic coefficients are computed in the form of analytical expressions as well as data tables. These are represented as

$$\begin{aligned} C_l &= c_0(\alpha, M, \mathbf{q}, \dot{\mathbf{q}}) + c_1(\alpha, M, \mathbf{q}, \dot{\mathbf{q}})\alpha \\ C_d &= d_0(\alpha, M, \mathbf{q}, \dot{\mathbf{q}}) + d_1(\alpha, M, \mathbf{q}, \dot{\mathbf{q}})\alpha \\ &\quad + d_2(\alpha, M, \mathbf{q}, \dot{\mathbf{q}})\alpha^2 \\ C_{m_{ac}} &= f_0(\alpha, M, \mathbf{q}, \dot{\mathbf{q}}) + f_1(\alpha, M, \mathbf{q}, \dot{\mathbf{q}})\alpha \end{aligned} \tag{1}$$

in which $\mathbf{q}$ and $\dot{\mathbf{q}}$ are arrays of nodal displacements and velocity vectors, respectively. Equation (1) represents a set of nonlinear aerodynamic coefficients including effects of blade motion and Mach number.

1. Coupled Trim Analysis

The coupled trim analysis consists of two phases, vehicle trim and steady response, calculated as one coupled solution using a modified Newton method. For a given flight condition, the control settings and the blade steady response must satisfy both the blade and the vehicle equilibrium conditions. The method of solving simultaneously the blade responses and the trim control settings is referred to as the coupled trim analysis. An uncoupled trim solution based on the rigid flapping blade assumption is used as an initial estimate for the coupled trim analysis. With the trim control settings, the blade steady responses are calculated. Using the blade responses, the rotor hub loads and a new vehicle equilibrium position are recomputed. The control settings are then updated based on the new equilibrium condition.

2. Vehicle Trim

Propulsive trim, which simulates an aircraft free flight condition, is used to calculate the initial rotor control settings. The solution is determined from the overall equilibrium equations (see Equation 2): three force (vertical Z, longitudinal X and lateral Y), and three moment (pitch, roll and yaw) equations. These are

$$
\begin{aligned}
F_1 &= F_{X_0}^H + D_F \cos\alpha_{HP} - T\sin\alpha_s = 0 \\
F_2 &= F_{Y_0}^H + Y_F \cos\phi_s - Y_{tr} + T\sin\phi_s = 0 \\
F_3 &= F_{Z_0}^H - T\cos\alpha_s\cos\phi_s - D_F\cos\phi_s\sin\alpha_{HP} \\
&\quad + Y_F\sin\phi_s = 0 \\
F_4 &= M_{X_0}^H + M_{x_F} + T\left(\bar{h}\cos\alpha_s\sin\phi_s - y_{cg}\cos\phi_s\right) \\
&\quad + Y_F\left(\bar{h}\cos\alpha_s\cos\phi_s + y_{cg}\sin\phi_s\right) = 0 \\
F_5 &= M_{Y_0}^H + M_{y_F} + T\left(\bar{h}\sin\alpha_s - x_{cg}\cos\alpha_s\right) \\
&\quad + D_F\left(-\bar{h}\cos\alpha_{HP} + x_{cg}\sin\alpha_{HP}\right) = 0 \\
F_6 &= M_{Z_0}^H + M_{z_F} - X_t Y_{tr} = 0
\end{aligned}
\tag{2}
$$

in which F_1, F_2, and F_3 are, respectively, the force equilibrium equations in the X, Y, and Z directions, and F_4, F_5, and F_6 are the rolling, pitching, and yawing moment equilibrium equations, respectively. Also, D_F is the fuselage drag; Y_F is the fuselage side force; Y_{tr} is the tail rotor thrust; T is the main rotor thrust; x_{cg} and y_{cg} and $\bar{h}$ are, respectively, the relative location of the rotor hub center with respect to the vehicle center of gravity in the X, Y, and Z directions; X_t is the nondimensional length (divided by rotor radius) between the main rotor hub and the tail rotor hub; and α_s and ϕ_s are the longitudinal and lateral shaft tilts, respectively (see Figure 2). Furthermore,

$$\alpha_s = \alpha_{HP} - \theta_{FP} \tag{3}$$

in which α_{HP} is the hub plane tilt relative to the flight direction, and θ_{FP} is the flight path angle relative to the longitudinal axis.

For a specified weight coefficient C_w, the unknown quantities to be determined from the vehicle equilibrium equations are

$$\mathbf{u}^T = \lfloor \alpha_s, \phi_s, \theta_{.75}, \theta_{1c}, \theta_{1s}, Y_{tr} \rfloor \ . \tag{4}$$

These values are recalculated iteratively using the modified hub forces and moments including the blade elastic responses. The solution technique is based on a modified Newton's method. The rotor controls, which are updated at the i^{th} iteration, can be expressed as

$$\mathbf{u_{i+1}} = \mathbf{u_i} + \mathbf{\Delta u_i} \tag{5}$$

in which

$$\Delta \mathbf{u_i} = - \left. \frac{\partial \mathbf{F}}{\partial \mathbf{u}} \right|_{\mathbf{u}=\mathbf{u_0}} \mathbf{F}(\mathbf{u_i}) \tag{6}$$

in which $\mathbf{u_0}$ are the trim control settings obtained initially using the rigid flapping blade solution, and the Jacobian $\partial \mathbf{F}/\partial \mathbf{u}$ is calculated using the finite difference approach. For computational efficiency, the Jacobian is computed only once initially and used for subsequent iterations.

3. Rotor Dynamic Response

The rotor dynamic response involves the determination of time-dependent blade positions at different azimuth locations for one rotor revolution. To reduce computational time, the finite element equations are transformed into modal space as a few normal mode equations using the coupled natural vibration characteristics of the blade. These nonlinear periodic coupled equations are solved for steady response using a finite element in time procedure based on Hamilton's principle in weak form [4]. One rotor revolution is divided into a number of azimuthal elements, and then periodicity of response is used to join the motions of the first and last elements. The assembly of elements results in nonlinear algebraic equations that are solved using the Newton-Raphson procedure.

After the blade response is obtained, hub forces and moments are calculated using the force summation method. These values are finally used to recalculate the coupled trim control values.

4. Rotor Wake Modeling

For the induced in-flow distribution on the rotor disk, a free wake model [5] is fully coupled in the rotor aeroelastic analysis. The model can account for wake self-distortion by updating its geometry according to newly calculated in-flow and blade circulation distributions. The geometry of the free wake is divided into three regions: near wake, rolling up wake, and far wake. The near wake consists of a series of radial panels, each with linear circulation distributions. The rolling up wake consists of an in-board linear circulation distribution panel, and a tip panel that represents the rolling up of the tip vortex. The far wake is modeled as one panel with a linear circulation distribution, and a concentrated tip vortex whose strength is proportional to the maximum circulation value on the rotor blade. The helical geometry of the concentrated tip vortex is updated while the in-board wake portions are not changed.

The free wake analysis is implemented in three stages. First, blade motion and loading are calculated using a linear in-flow model. Next, wake-induced coefficients are calculated for an undistorted wake geometry. The nonuniform in-flow is calculated and is used to obtain blade motion and loading. Finally, the free wake geometry is calculated. For this, the influence coefficients are re-evaluated, and blade motion and loading are again obtained using nonuniform in-flow values. For subsequent iterations, the free wake geometry is generally held fixed, and only the strength of vortices is updated.

III. Solution Procedure

The following procedure was used to study the simulated ballistic damaged effects on helicopter rotor response and loads in forward flight conditions.

1. With prescribed input data, vehicle trim equations are calculated using rigid blade flapping (a starting point).

2. Using control inputs from the vehicle trim solution of Step 1 and prescribed blade damage condition, the blade nonlinear steady response is calculated. The results give detailed individual blade responses at different span-wise and azimuthal positions.

3. Hub loads and moments are calculated using elastic rotor responses. Then, the vehicle trim values and blade responses are recalculated iteratively using the modified hub forces and moments. This step is repeated until a converged solution is obtained.

4. Steps of 2 to 3 are repeated for different damage configurations.

IV. Results and Discussion

Numerical results are first calculated for a undamaged (baseline) rotor of the SA349/2 Gazelle helicopter for level flight conditions. Results then are calculated for this rotor with simulated damaged conditions and the effects of blade damages are assessed. Some of important structural and aerodynamic characteristics of this helicopter rotor are given in Table 1. Other characteristics of this helicopter are given in Reference 6.

The SA349/2 Gazelle helicopter was fitted with an advanced geometry three-bladed articulated rotor. The Grande Vitesse (GV) blades consisted of OA209 advanced airfoils (9% thickness ratio), adjustable tips, and nonlinear twist distributions.

In the present study, an effort was made to model the helicopter blade characteristics as accurately as possible. The structural properties of blades obtained from the measured data [6] were used for blade finite element model (see Table 2). Nonlinear twist distribution of the blade was also modeled in the blade finite elements. One of the main features in this articulated rotor blade is a lag damper. The lag damper can significantly affect the blade dynamics. In the present analysis, additional stiffness as well as damping terms attributable to the lag damper were included.

For the calculation of blade dynamic response, each rotor blade is discretized into eight beam elements, and each beam element consists of 15 nodal degrees of freedom. For normal mode reduction, five coupled rotating natural modes are used, comprised of two flaps, two lags, and one torsion mode. For periodic response, one cycle of time is discretized into eight time elements, and each time element represents a fifth order polynomial distribution of motion.

Table 1: SA349/2 Gazelle Helicopter Characteristics.

Aircraft gross weight	4400 lbs
Number of blades, N_b	3
Radius, R	17.5 ft
Blade chord, c	1.17 ft
Solidity, σ	0.064
Lock number, γ	5.13
Rotor thrust ratio, C_T/σ	0.064
Blade airfoil	OA209
Rotational speed, Ω	387 rpm
Rotating flap natural frequency	1.02/rev
Rotating lag natural frequency	0.49/rev
Rotating torsion natural frequency	4.28/rev
Fuselage lift coefficient, C_{L_f}	0.00499
Fuselage drag coefficient, C_{D_f}	0.0092
Fuselage pitch moment , C_{m_f}	-0.00086
Fuselage roll moment , C_{l_f}	-0.0001
Fuselage yaw moment , C_{n_f}	0.0001

Table 2: Structural Properties of Gazelle Rotor Blade.

Element Number	$\frac{EI_y}{m_0\Omega^2R^4}$	$\frac{EI_z}{m_0\Omega^2R^4}$	$\frac{GJ}{m_0\Omega^2R^4}$	$\frac{m}{m_0}$	$\frac{l_i}{R}$
1 (tip)	.000781	.08847	.000724	0.5900	.1000
2	.000494	.02600	.001800	1.7796	.1000
3	.000620	.03178	.001184	0.7796	.1760
4	.000608	.03943	.001077	0.7755	.1015
5	.000597	.03943	.001077	0.7755	.1015
6	.000012	.04554	.000964	0.8129	.2124
7	.003862	.01720	.052152	3.6113	.1181
8 (root)	.051004	.24291	.070430	7.8198	.0695

1. Baseline (Undamaged) Helicopter: Correlation Study

To validate the coupled trim procedure used in the present study, calculated trim values of baseline (undamaged) helicopter are correlated with existing flight test data [6] for four level flight conditions (advance ratio $\mu = 0.14, 0.256, 0.333, 0.378$).

Figure 3 shows the correlation of the power requirement to maintain the level flight of the helicopter. The torque coefficient (C_Q) obtained from the coupled trim solution was used to calculate shaft power. The quasi-steady aerodynamics with the free wake model are used for the entire flight envelope. Excellent correlations with flight test data are observed.

The blade flapping angles are also correlated with flight data and shown in Figures 4 through 6. Calculated blade flap responses at the tip, in terms of the coning angle (β_0) and the rotor disk tilt angles (β_{1c}, β_{1s}), are compared with the data for four flight conditions. Reasonably good agreement with test data was observed, providing the author with a certain confidence in the helicopter rotor subsystem model constructed in the present study.

In the following section, results are calculated for the helicopter damaged on its rotor blade, and then blade damage effects on blade and hub loads are assessed.

2. Helicopter with Damaged Blade

Blade ballistic damage is simulated as a reduction in structural properties as well as a change in aerodynamic characteristics of blade. The structural damage is simulated as a 50% reduction in bending and torsional stiffness (EI_y, EI_z, and GJ) and mass of damaged blade section. The aerodynamic damage is simulated as a change in blade aerodynamic characteristics in terms of section lift, drag, and moment coefficients. In the present study, the following relations are used:

$$\begin{aligned} C_{l\text{damage}} &= \beta_l \, C_{l\text{undamaged}} \\ C_{d\text{damage}} &= \beta_d \, C_{d\text{undamaged}} \\ C_{m_{ac}\text{damage}} &= \beta_m \, C_{m_{ac}\text{undamaged}} \end{aligned} \tag{7}$$

in which $\beta_l, \beta_d, \beta_m$ are respectively the lift, drag, and moment deficiency functions. The values used in the present study are summarized in Table 3. These are estimated based on the wind tunnel test results. The details of test, including data acquisition and reduction, are available in Reference 2.

Table 3: Aerodynamic Deficiency Functions of Damaged Airfoil.

Deficiency Functions	$M_{inc} \leq 0.7$	$M_{inc} > 0.7$
β_l	0.75	$\frac{0.75}{\sqrt{1-M^2}}$
β_d	2.5	$\frac{2.5}{\sqrt{1-M^2}}$
β_m	0.9	$\frac{0.9}{\sqrt{1-M^2}}$

Table 4: Frequencies of Damaged Blades (per rev).

Mode	Baseline	Damage 1	Damage 2
First Lag	0.492	0.575	0.856
First Flap	1.016	1.048	1.181
Second Flap	2.694	2.783	2.923
First Torsion	4.289	4.460	4.438
Second Lag	4.611	4.768	5.056

In the present study, two different blade damage conditions are considered: Damage 1 and Damage 2. Damage 1 represents a condition in which 10% of the outboard blade tip of one blade is damaged, resulting the reduction in structural and aerodynamic capability of that blade section. Damage 2 represents a more severe damage condition, in which 20% of the outboard section is damaged (see Figure 7).

Effects of the simulated damages on the blade natural frequencies are summarized in Table 4, and the corresponding mode shapes are shown in Figures 8 through 12. The results of baseline (undamaged) blade are shown, along with two damage cases. It is shown that the blade damage affects all the modes of the blades. Of particular interest is the behavior of the fundamental lag frequency of the blade, since the lag motion is very important in blade dynamic study. As the size of the damage (%) increases, the frequency of the first lag mode is increased. This is thought to be caused by changes in the centrifugal force due to blade mass/stiffness effects. The torsional mode shape of the 20% tip damaged blade (Damage 2) is quite different from that of baseline and Damage 1 (see Figure 12). This is because of a large coupling effect between the second lag and the first torsional modes.

Most of the comprehensive aeroelastic codes developed to calculate helicopter flight dynamic response and stability employ the assumption that the response of all the blades is identical with an appropriate phase shift for each blade. Thus, in the rotor response calculation, a set of coupled flap-lag-torsion equations corresponding to a single blade is used. In the study of ballistically damaged rotor subsystems, the motion of each blade has to be represented by an independent set of equations, and their response is calculated individually. This type of solution approach is referred as a "multi-blade formulation." This formulation also drastically increases the size of equations to be solved. For example, the size of system equations quadruples for a four-bladed rotor. In the present study, a multi-blade formulation proposed by Chopra [7] is used to calculate the rotor hub forces and moments. Therefore,

the motions of the individual blades are considered in the following discussion of results.

Figures 13 through 15 present the time histories of hub loads (nondimensionalized by $m\Omega^2R^2$) transferred to the airframe. Again, for comparison purposes, the results of undamaged rotor system are shown, along with the two damage cases for a high speed flight condition ($\mu = 0.338$): Figures 13 and 14 for the in-plane hub loads and Figure 15 for the out-of-plane loads. These forces were calculated using a multi-blade formulation considering the motions of all the blades. These forces cause vehicle vibration and are very important for establishing control margins. One observes the 3/rev variation of forces with this three-bladed rotor for the undamaged (baseline) case. One also observes a significant increase in the magnitude of all three force components as the amount of damage increases (Damage 2 case). It is also interesting to note that the vertical force variation of Damage 1 is quite different from that of Damage 2, as shown in Figure 15. This points out the importance of nonlinear aeroelastic analysis for damaged helicopter rotor subsystems: One may not simply apply aeroelastic vulnerability data linearly to similar damage cases.

V. Conclusions

Simulated ballistic damage effects on helicopter rotor blade response and rotor hub loads are investigated using a comprehensive aeroelastic analysis. The analysis is based on finite element theory in space and time coordinates. Each blade is treated as an elastic beam undergoing combined flap-lag-torsional motions. Multi-blade formulation is used to calculate the forces and moments acting on the rotor hub. Results are calculated for the baseline undamaged rotor system of SA 349/2 Gazelle helicopter and with two simulated blade damage conditions. Based on the analysis results, the following conclusions are drawn from this study:

1. Blade damage affects all the modes of the blade. The effects are more distinct in the higher modes.

2. As the amount of blade damage increases, the fundamental frequency of the lag mode is increased.

3. Blade dissimilarity induces a large 1/rev variation in the hub loads.

Recommendation for future study

From this study, it was shown that a 20% rotor blade tip damage would induce a severe vibration in the study aircraft primarily because of large rotor blade dissimilarity. This will most likely limit the helicopter's flight performance in terms of the vehicle's mobility. This severe vibration, however, will also affect the aircraft's dynamic stability and control. Future study of investigating these phenomena would be of great interest.

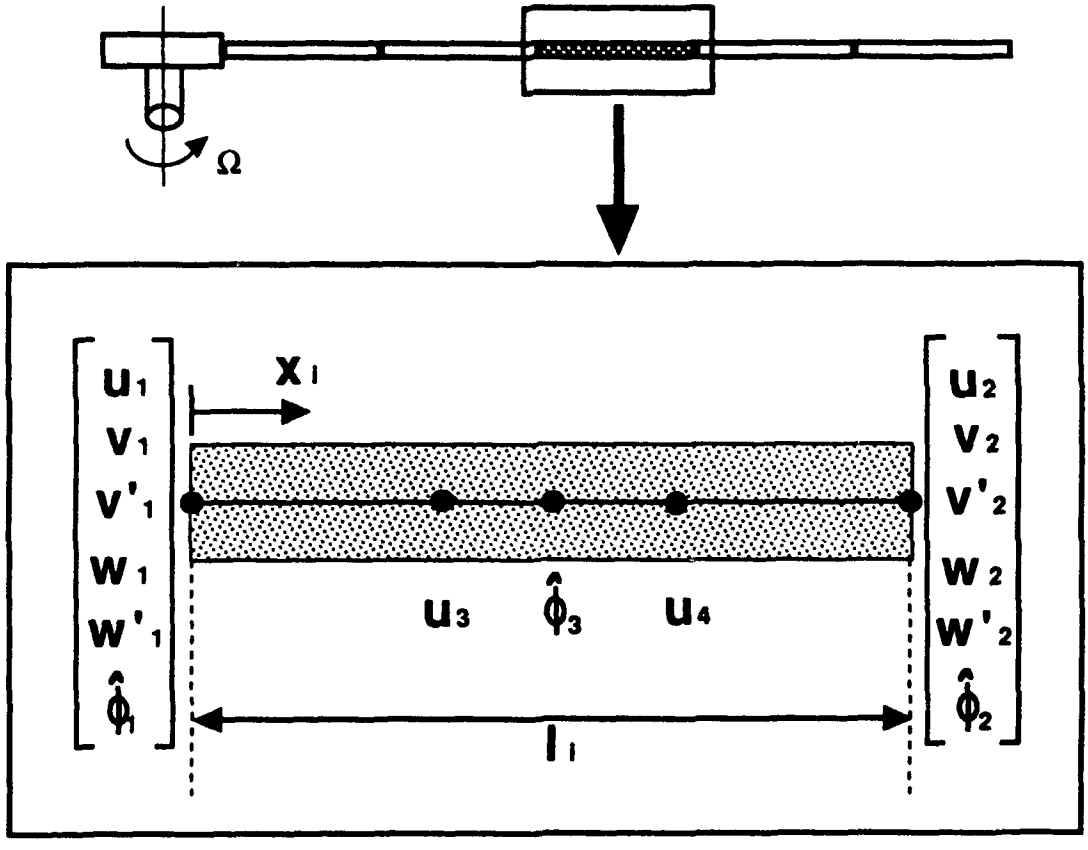

Figure 1: Finite Element Model of a Helicopter Rotor Blade.

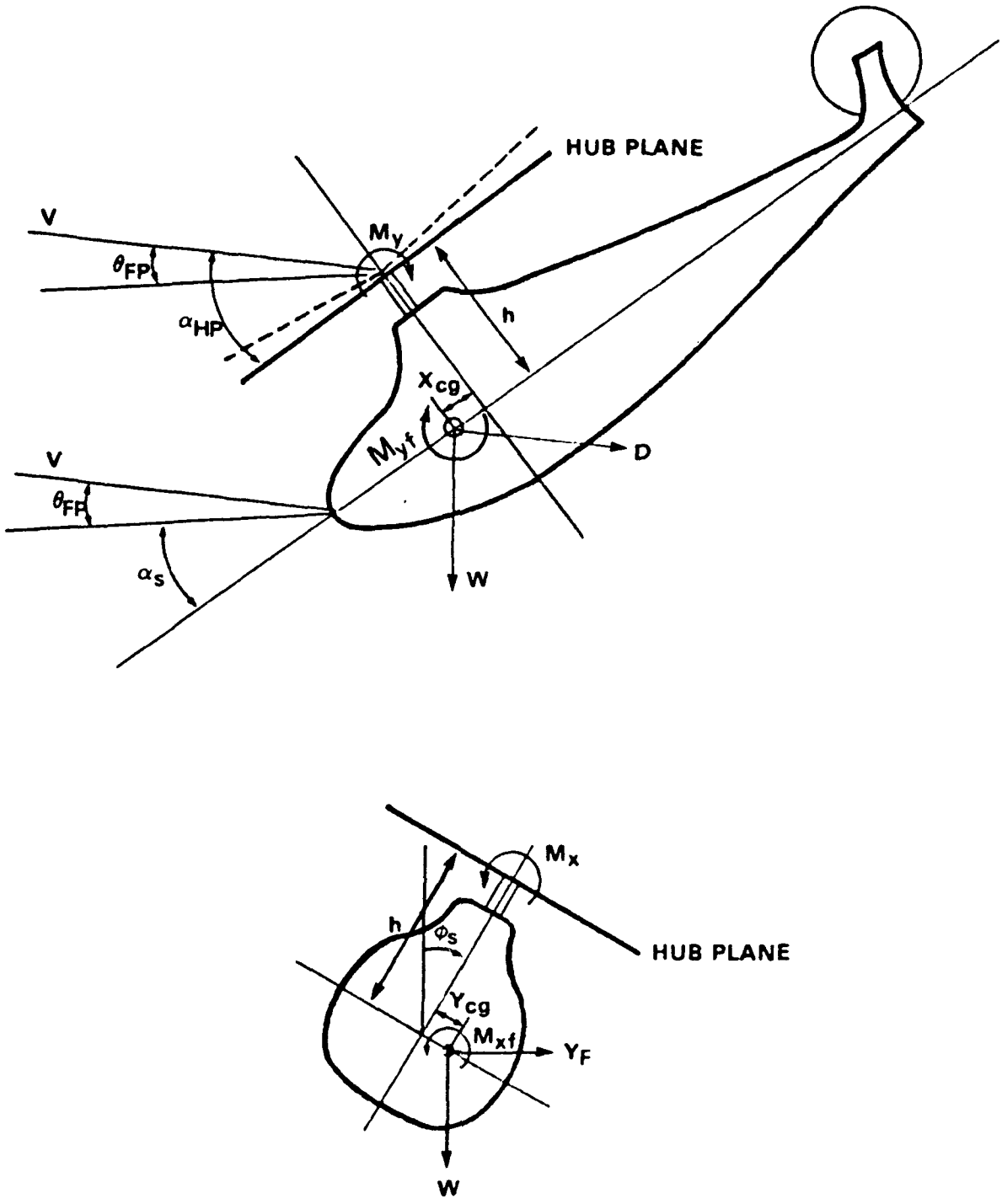

Figure 2: Schematic of Rotor-Vehicle Diagram.

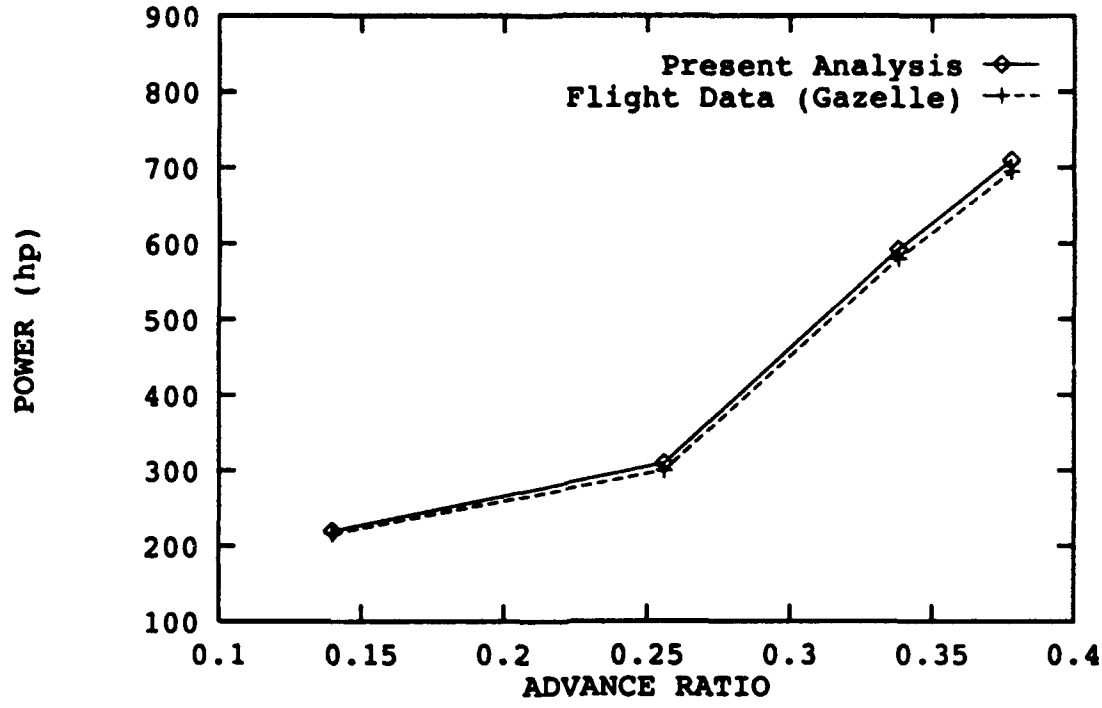

Figure 3: Correlation of SA349/2 Shaft Power.

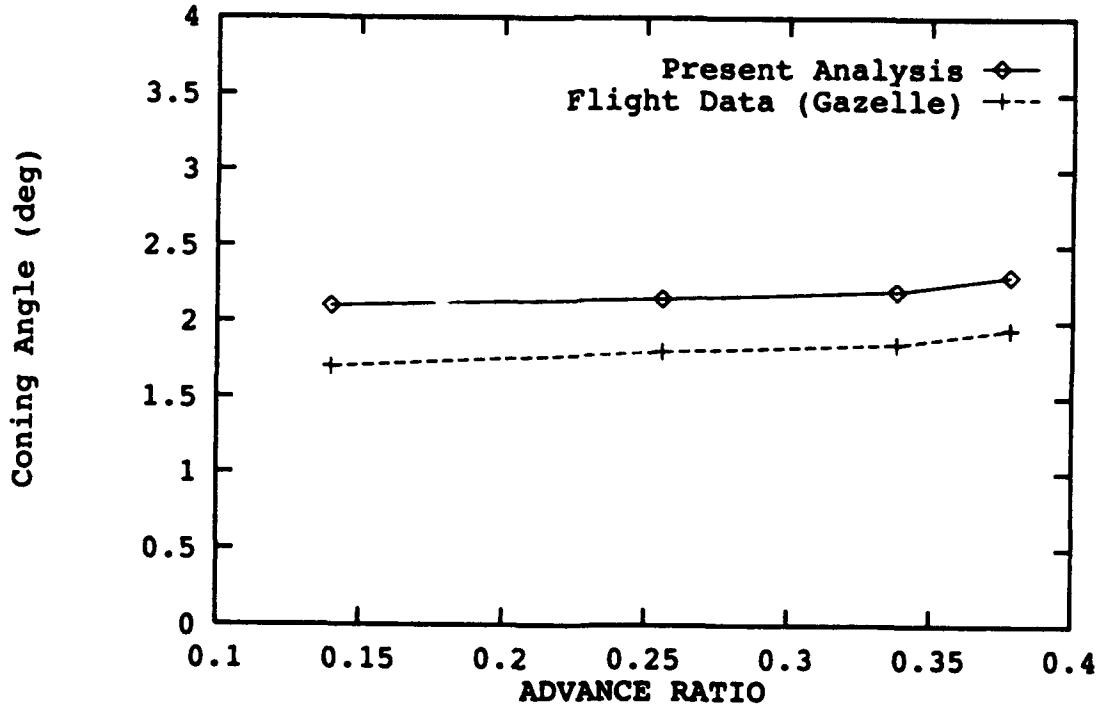

Figure 4: Correlation of Flap Response - Coning Angle β_0.

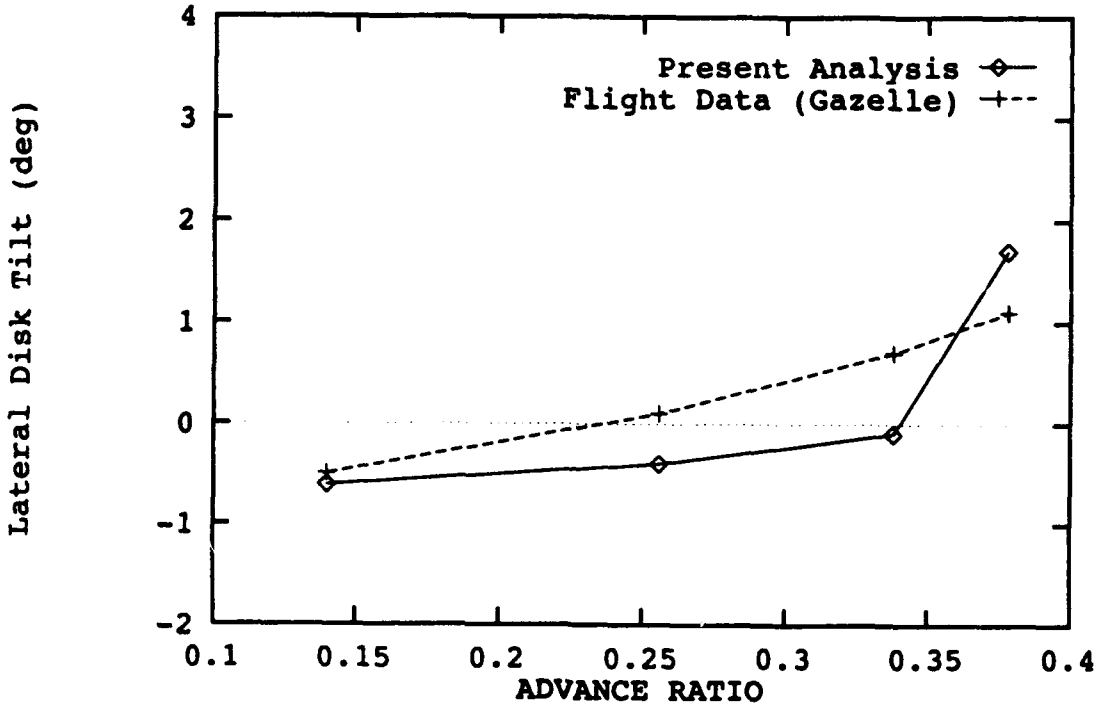

Figure 5: Correlation of Flap Response - Lateral Disk Tilt β_{1s}.

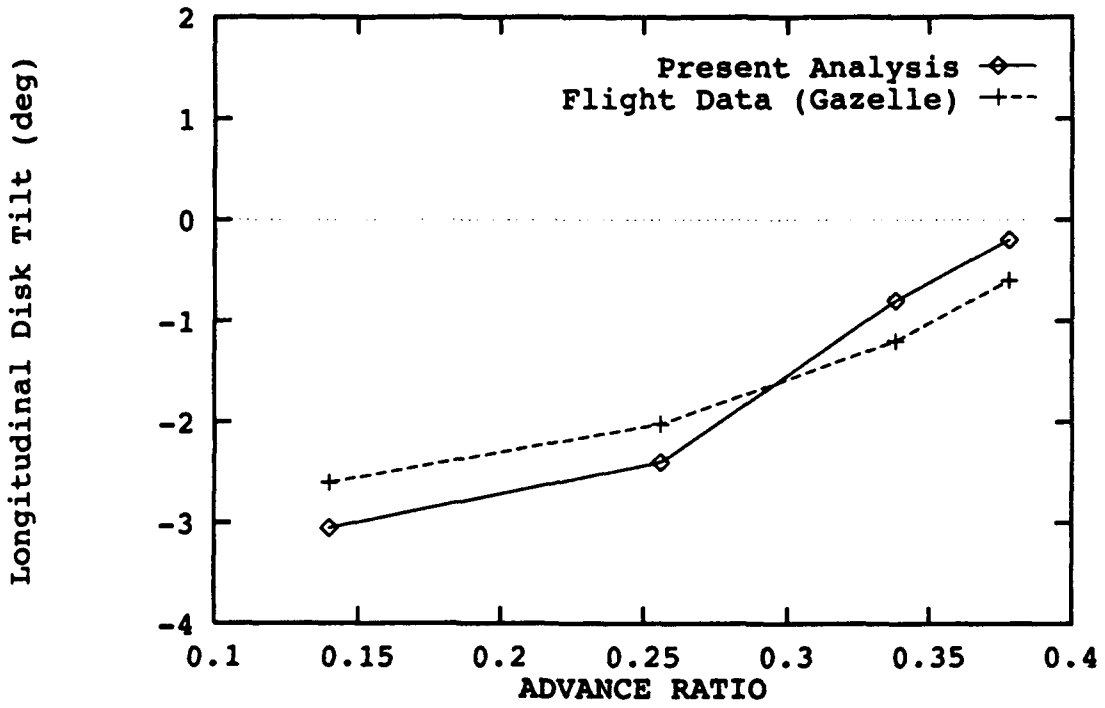

Figure 6: Correlation of Flap Response - Longitudinal Disk Tilt β_{1c}.

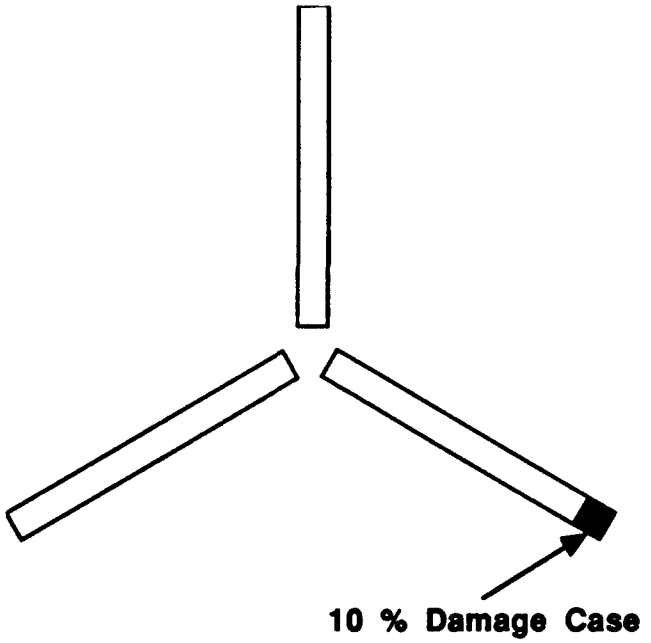

a) Damage 1

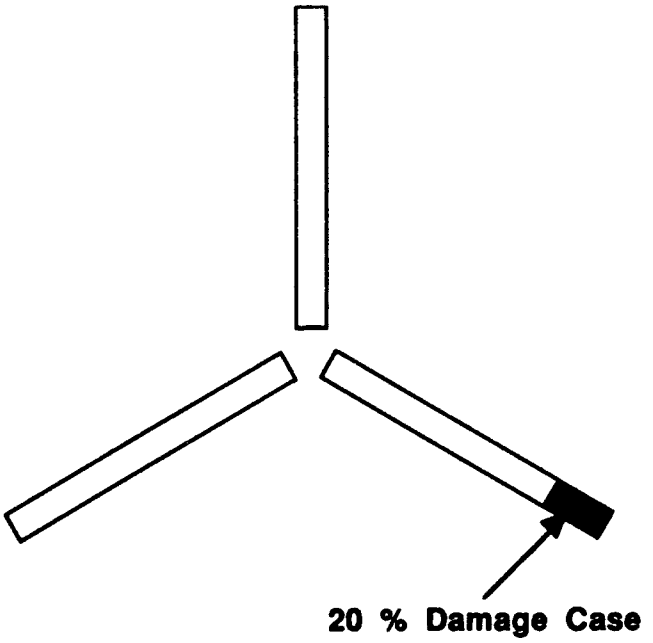

b) Damage 2

Figure 7: Schematic of Blade Damage Cases.

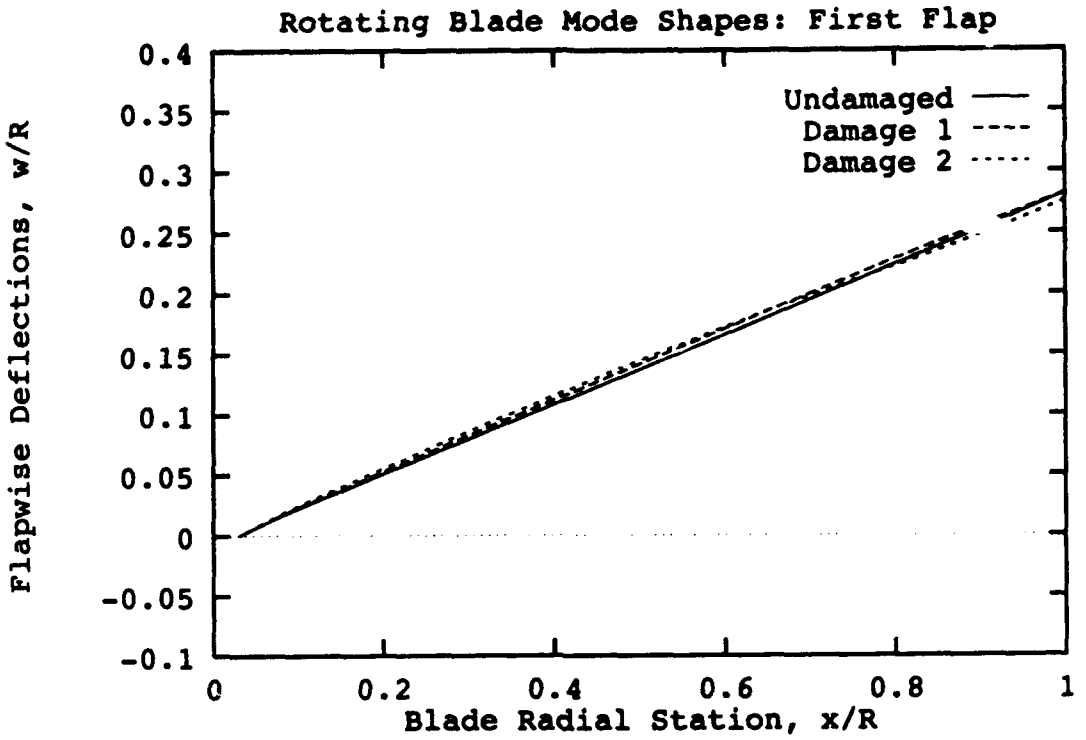

Figure 8: First Flap Mode Shapes of Undamaged and Damaged Blades.

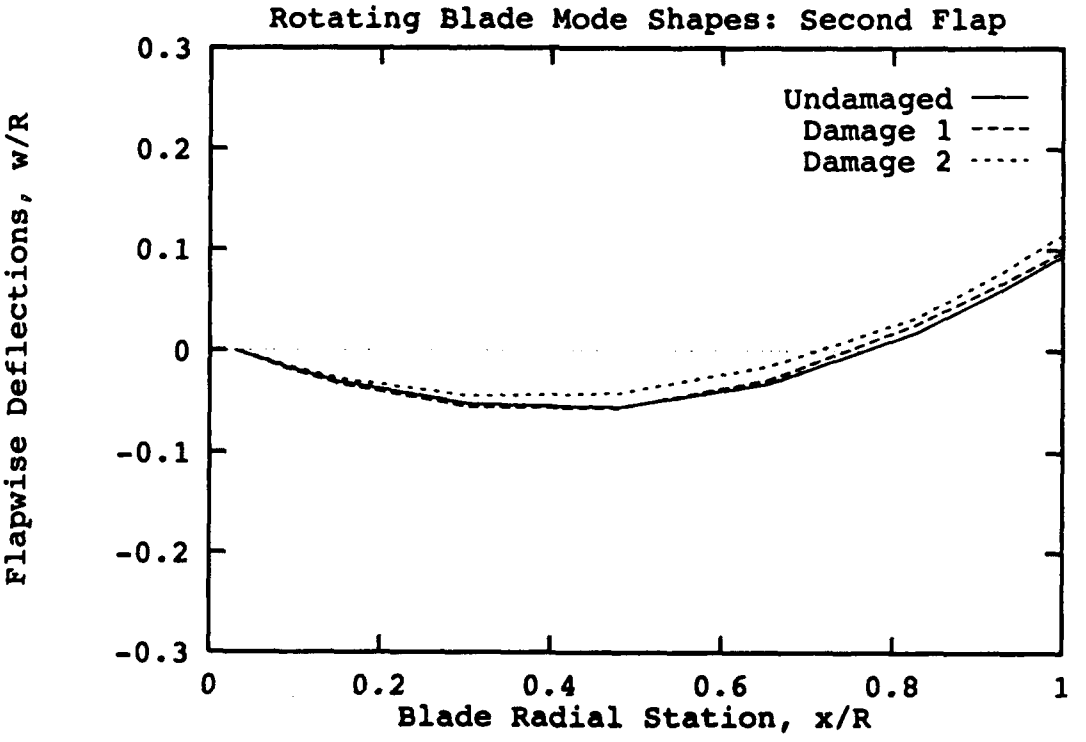

Figure 9: Second Flap Mode Shapes of Undamaged and Damaged Blades.

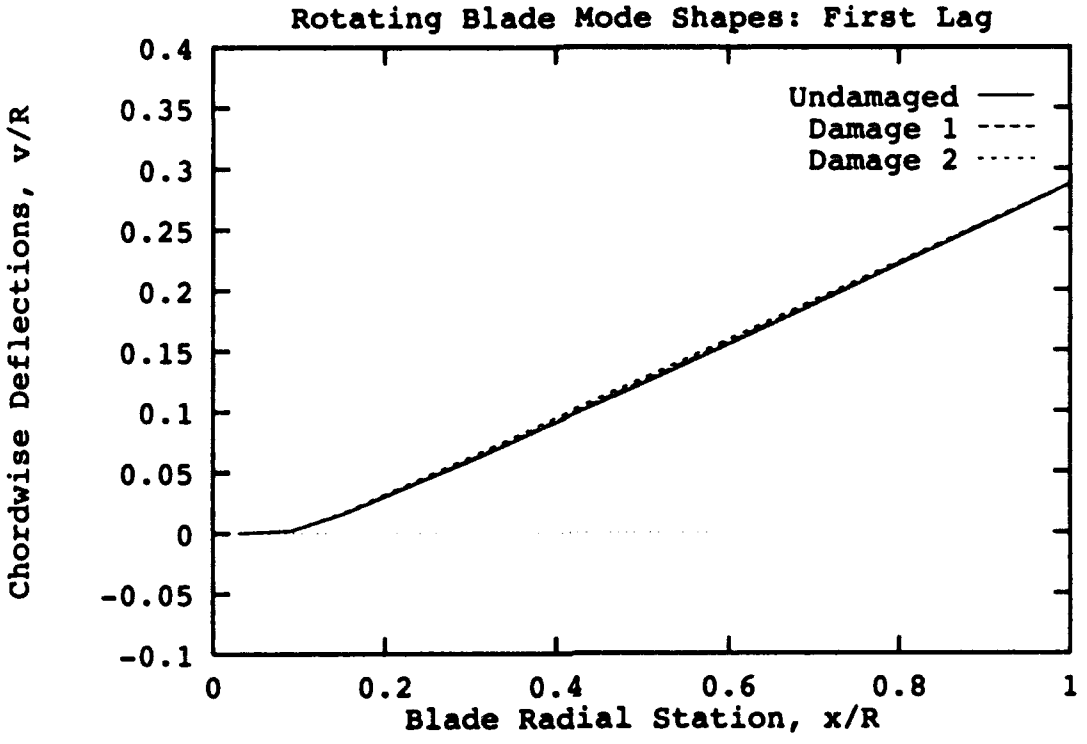

Figure 10: First Lag Mode Shapes of Undamaged and Damaged Blades.

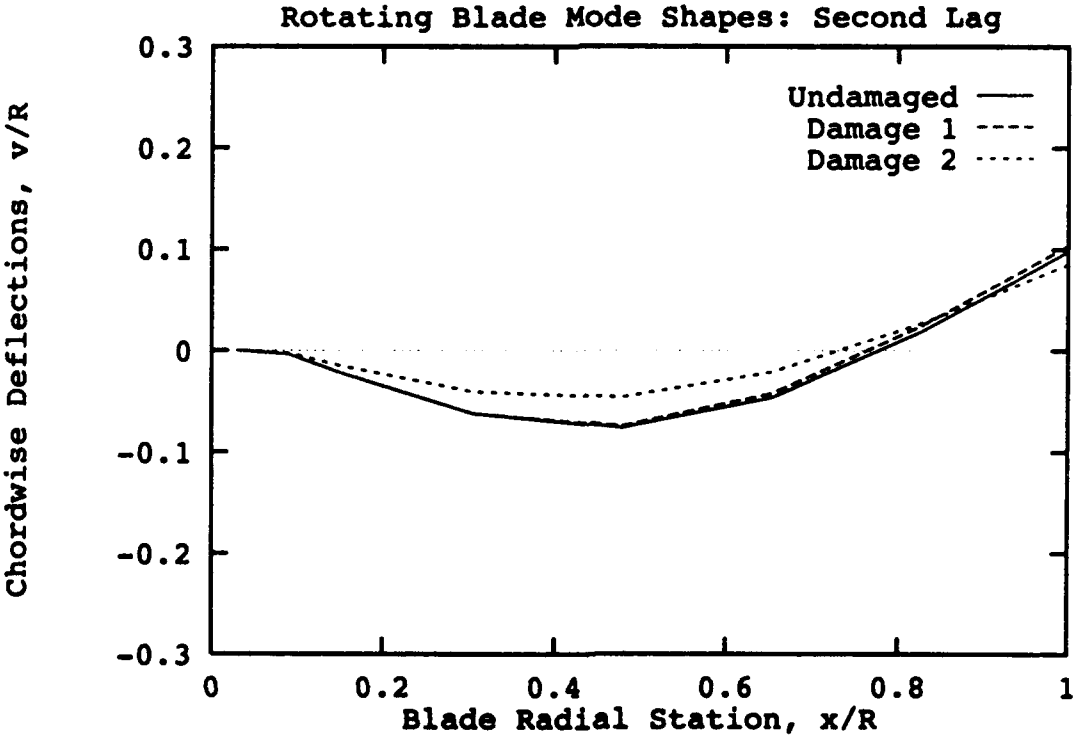

Figure 11: Second Lag Mode Shapes of Undamaged and Damaged Blades.

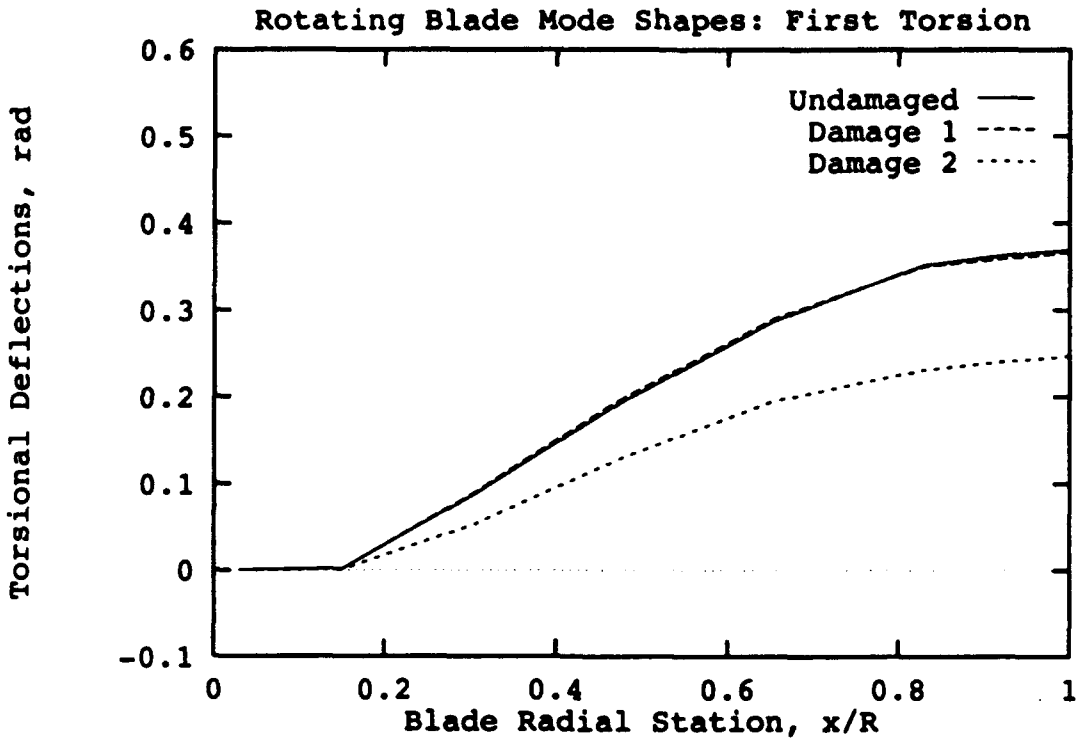

Figure 12: Torsional Mode Shapes of Undamaged and Damaged Blades.

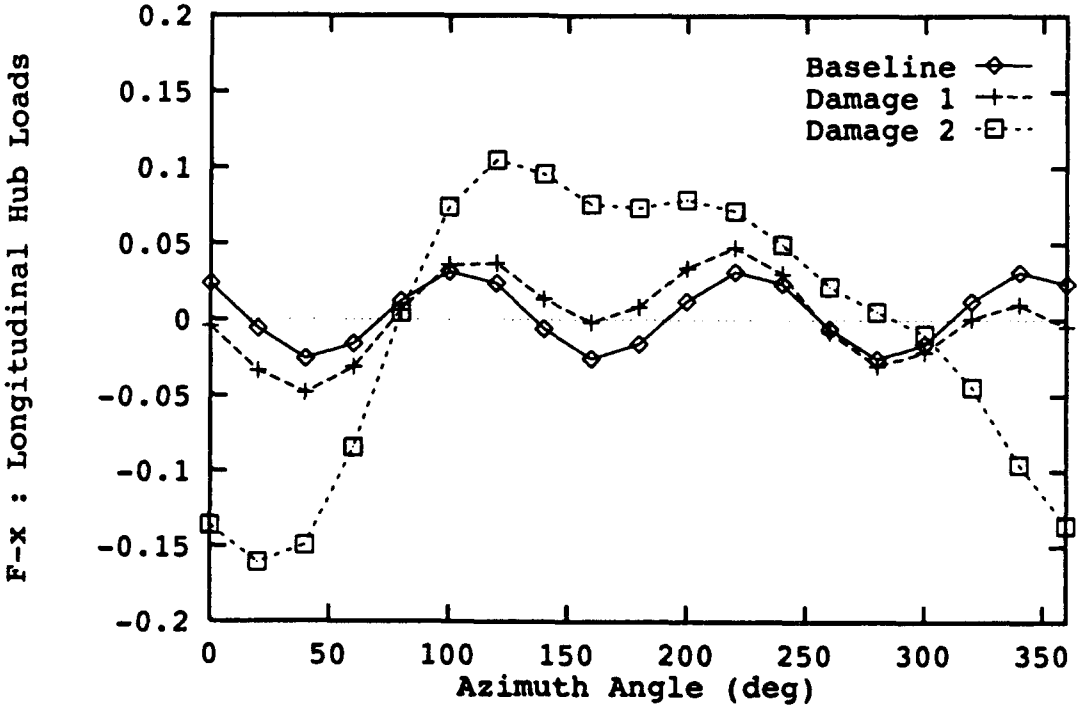

Figure 13: Variations of Longitudinal In-Plane Hub Loads ($\mu = 0.338$).

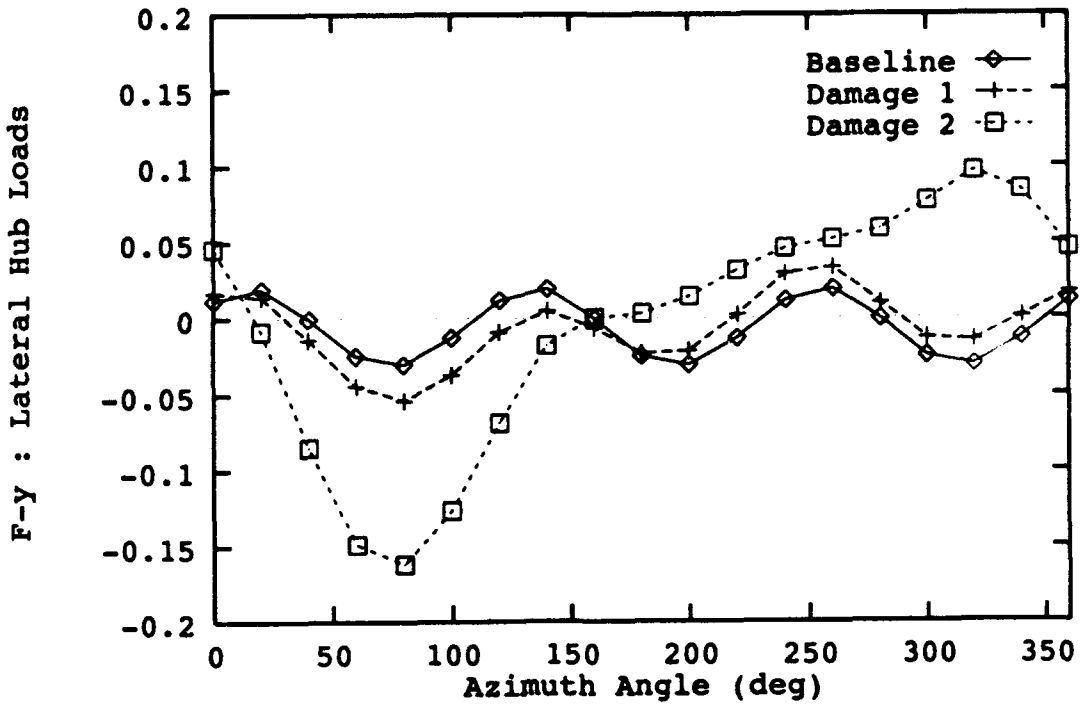

Figure 14: Variations of Lateral In-Plane Hub Loads ($\mu = 0.338$).

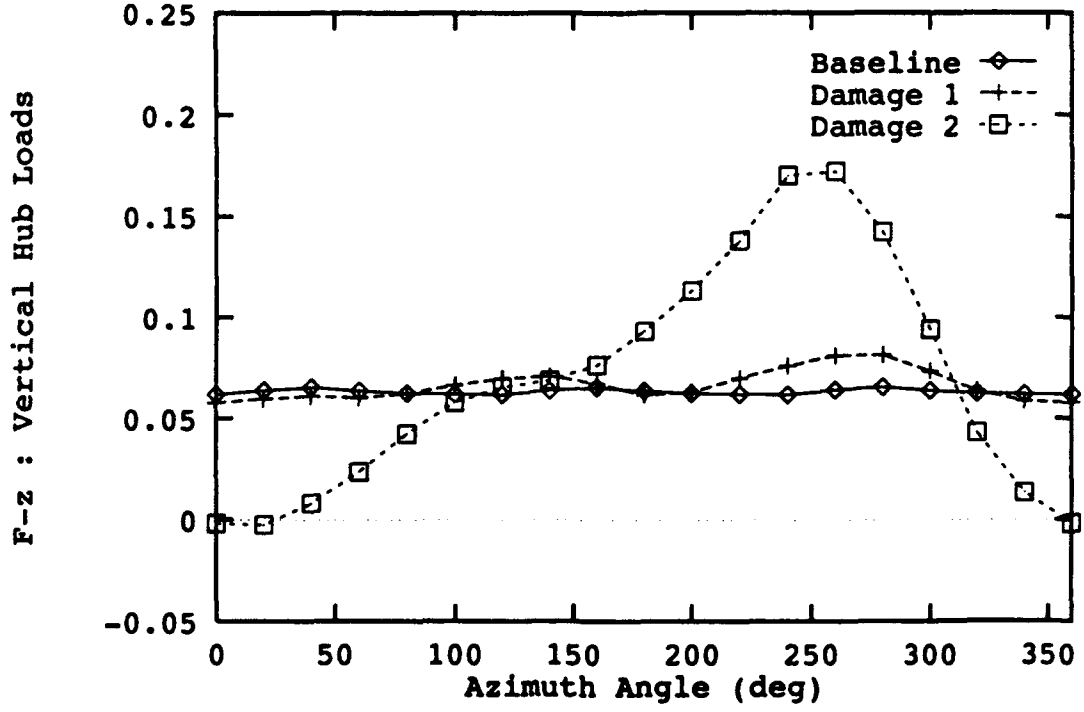

Figure 15: Variations of Out-of-Plane Hub Loads ($\mu = 0.338$).

VI. References

[1] Bir, G., I. Chopra, and K. C. Kim *et al.* "University of Maryland Advanced Rotorcraft Code (UMARC): Theory Manual." Technical Report 92-02, Aerospace Engineering Department, University of Maryland, College Park, MD, May 1992.

[2] Leishman, J. G. "Aerodynamic Characteristics of a Helicopter Rotor Airfoil As Affected by Simulated Ballistic Damage." Army Research Laboratory Contractor Report, ARL-CR-66, Aberdeen Proving Ground, MD, September 1993.

[3] Johnson, W. "A Comprehensive Analytical Model of Rotorcraft Aerodynamic and Dynamics." NASA Technical Memorandum (TM) No. 81182, NASA Ames, CA, June 1980.

[4] Panda, B. and I. Chopra. "Dynamics of Composite Rotor Blades in Forward Flight." Vertica, vol. 11, no. 1, January 1987.

[5] Johnson, W. "Assessment of Aerodynamic and Dynamic Models in a Comprehensive Analysis for Rotorcraft." Computers and Mathematics with Applications, vol. 12A, no. 1, January 1986.

[6] Heffernan, R. M. and M. Gaubert. "Structural and Aerodynamic Loads and Performance Measurements of an SA349/2 Helicopter with an Advanced Geometry Rotor." NASA Technical Memorandum (TM) No. 88370, NASA Ames, CA, November 1986.

[7] Chopra, I. "Helicopter Dynamics and Aeroelasticity." Technical Notes, Center for Rotorcraft Education and Research, Aerospace Engineering Department, University of Maryland, College Park, MD, January 1991.

INTENTIONALLY LEFT BLANK.

Appendix A

UMARC Input Data Set

Flight Condition Inputs

Advance ratio, μ.

Rotor speed ratio, Ω/Ω_o : Ω_o is a nominal rotor rpm.

Density ratio, ρ/ρ_o : ρ_o is a standard sea-level air density.

Flight angle, θ_{FP} (rad).

Tip Mach number, M_{tip}.

Main Rotor Overall Configuration Inputs

Rotor type (articulated or hingeless or bearingless).

Number of blades, N_b.

Solidity, σ

Lock number, γ.

Rotor thrust ratio, C_T/σ.

Hub location (x,y,z) with respect to aircraft c.g.

Main Rotor Blade Configuration Inputs

Linear twist, θ_{tw} (rad): positive for leading edge up.

Precone, β_p (rad): negative for droop.

Root cutout, R_{root}.

Number of spatial beam elements, n.

Blade Element Structural Properties Inputs : required for each n elements.

Element length, l_i.

Chord length, c.

Element mass, m.

Chord-wise offset of tensile axis ahead of elastic axis, e_a.

Chord-wise offset of aerodynamic center behind elastic axis, e_d.

Chord-wise offset of blade center of mass ahead of elastic axis, e_g.

Axial stiffness, EA.

Section stiffness constants, EB_1, EB_2.

Warping rigidity, EC_1.

Section warping constant, EC_2.

Flap-wise bending stiffness, EI_y.

Lag (Chord-wise) bending stiffness, EI_y.

Torsional stiffness, GJ.

Radius of gyration of blade cross section, k_A.

Blade cross-sectional mass radius of gyration, k_m.

Blade cross-sectional mass radius of gyration in flap direction, k_{m_1}.

Blade cross-sectional mass radius of gyration in lag direction, k_{m_2}.

Blade sweep angle, θ_{sw} (rad): negative for swept back.

Blade droop angle, θ_{dr} (rad): negative for droop down.

Tail Rotor Configuration Inputs

Tail rotor radius ratio, R_{tr}/R : R is a main rotor radius.

Tail rotor gear ratio, Ω_{tr}/Ω : Ω is a main rotor rpm.

Tail rotor blade twist, θ_{tw} (rad): positive for leading edge up.

Number of blades, N_{b_t}.

Solidity, σ_t.

Tail rotor hub location (x,y,z) with respect to aircraft c.g.

Mean lift curve slope, $c_{l_{tr}}$.

Mean chord length, c_{tr}.

Horizontal Tail Configuration Inputs

Horizontal tail area ratio, S_{ht}/A: A is a main rotor disk area (πR^2).

Longitudinal distance between aircraft c.g. and tail aerodynamic center, x_{ht}.

Mean lift curve slope, $c_{l_{ht}}$.

Mean chord length, c_{ht}.

Fuselage Configuration Inputs

Effective fuselage mass, M_f.

Fuselage roll inertia, I_ϕ.

Fuselage pitch inertia, I_α.

Fuselage lift coefficient, C_{L_f}.

Fuselage drag coefficient, C_{D_f}.

Fuselage parasite drag area, f/A.

Fuselage side force coefficient, C_{Y_f}.

Fuselage pitch moment coefficient, C_{m_f}.

Fuselage roll moment coefficient, C_{l_f}.

Fuselage yaw moment coefficient, C_{n_f}.

INTENTIONALLY LEFT BLANK.

Appendix B

Sample Gazelle Input Data

```
  title  :   gazelle rotor  ( sa349/2 helicopter )
!            us aero     5 fuselage dof          dynamic inflow
!                      (stability analysis)
*-------------------------------------------------------------------
  rotor_properties

! rotor_type :  articulated          flap_lag_delta3
! rotor_name :  gazelle
! no_blades              =  3        solidity                =  0.064
! lock_no                =  5.5      ct/sigma                =  0.065
! cg_below_hub           =  0.25
! cg_hub_offset_x        =  0.017    cg_hub_offset_y         =  0.0

*-------------------------------------------------------------------
  blade_properties

! twist(deg)              =  0.       precone(deg)              =  0.0
! lag_spring_constant   = 0.0663     lag_damper_constant     = 0.0151
! delta3_constant       = 0.0294     pitch_spring_constant   = 0.0150
! root_cut(%)            =  10.0     no_space_elements         =    8


!  element_length :   0.100000   0.100000  0.176000   0.101500
!                     0.101500   0.212400  0.118100   0.069500

!  chord          :   0.0667     0.0667    0.0667     0.0667
!                     0.0667     0.0667    0.0667     0.0667

!  eiy            :   0.000781   0.000494  0.000620   0.000608
!                 :   0.000597   0.000012  0.003862   0.051004

!  eiz            :   0.088477   0.026000  0.031780   0.039430
!                 :   0.039430   0.045540  0.017200   0.242910

!  gj             :   0.000724   0.001800  0.001184   0.001077
!                 :   0.001077   0.000964  0.052152   0.070430

!  ea             :   50.0       50.0      50.0       50.0
!                 :   50.0       50.0      50.0       50.0


!  offset_cg&ea   :     0.023  -0.003   -0.023   -0.026
!                     -0.029  -0.056    0.0      0.0

!  offset_ta&ea   :     0.0  0.0  0.0  0.0  0.0  0.0  0.0  0.0

!  offset_ac&ea   :    -0.060  -0.060    0.057    0.057
!                      0.057   0.010    0.0      0.0
```

```
!  sq_km2          :   0.000381   0.000180    0.000248    0.000248
!                  :   0.000248   0.000249    0.000155    0.000544

!  sq_km1          :   0.0000110  0.0000040   0.0000030   0.0000030
!                  :   0.0000030  0.0000170   0.0000001   0.0001090

!  pl_chord_length  =  0.01
!  pl_axial_length  =  0.01                pl_height  =  0.02

*-------------------------------------------------------------------

   fuselage_properties

!      no_hub_dof = 5

!      body_seq       :   1  2  3  4  5

!      effective_x_mass        = 86.1
!      effective_y_mass        = 86.1
!      effective_z_mass        = 86.1
!      fuselage_pitch_inertia = 10.2709
!      fuselage_roll_inertia  = 1.7681


*-------------------------------------------------------------------

   tail_properties

!  gear_ratio_tail_rot    = 15.2
!  solidity_tail_rot      = 0.4644
!  rad_ratio_tail_rot     = 0.0662
!  cg_tail_rot_offset_x   = 1.1162
!  tail_rot_above_cg      = 0.0933
!  twist(deg)_tail_rot    = 0.0
!  cl_tail_rot            = 5.7

!  area_ratio_tail_hor    = 0.0
!  cg_tail_hor_offset_x   = 1.0
!  cl_tail_hor            = 4.5
!  c0_tail_hor            = 0.0

*-------------------------------------------------------------------

   airfoil_properties

! airfoil = myairfoil

! table_look_up  : on     no_airfoils  =  1
! airfoil_starting_locations = .0
! cl_table_names  test
! cd_table_names  test
! cm_table_names  test
```

```
! ref_lift_curve_slope  =  6.00
! le_recov_fact  =  0.97

*-------------------------------------------------------------------

   flight_condition

!   advance_ratio      =  0.338      density_ratio =    1.0
!   rotor_speed_ratio =  1.0
!   tip_mach           = 0.65      flight_angle  =    0.0

*-------------------------------------------------------------------

   aerodynamics

*      uniform_inflow
*      drees_linear_inflow

!      reverse_flow

!      l_circ_us

*      l_us_drag
*      l_us_pm

*      l_impul_us

*      nl_us_te_sep

!      dyn_stall

*      sing_peak_pres_wake

!      sing_peak_free_wake

*      dual_peak_pres_wake

*      dual_peak_free_wake

!      free_wake_iter_no = 9

*-------------------------------------------------------------------

   trim_analysis

*  coupled_rb

!  nl_struct_aero
!  first_flap_freq      =  1.016
```

```
*  coupled_trim_scheme  =      newton
!  coupled_trim_scheme  = marq_newton
!  delta_controls(%)    :  5

!  conv_crit            :  active
!  resp_conv_crit       = 0.005
!  trim_conv_crit       = 0.0001

!  no_max_iter          =  50
!  qs_aero_damp         =  40.00
!  us_aero_damp         =  40.00

!  no_time_elements     = 8
!  nodes_per_time_elem  = 6

!  no_flap_modes = 2
!  flap_mode_seq = 2   3

!  no_lag_modes  = 2
!  lag_mode_seq  = 1   6

!  no_torsion_modes  = 1
!  torsion_mode_seq  = 4

!  no_axial_modes  = 0
!  axial_mode_seq  = 10

*-------------------------------------------------------------------

  stability_analysis

!  fix_qs_const
!  no_psi_locations = 24
!  dynamic_inflow

*-------------------------------------------------------------------

   output_options     print_control    =  4
!                     hub_load_control =  0

*-------------------------------------------------------------------
```

No. of Copies	Organization
2	Administrator Defense Technical Info Center ATTN: DTIC-DDA Cameron Station Alexandria, VA 22304-6145
1	Commander U.S. Army Materiel Command ATTN: AMCAM 5001 Eisenhower Ave. Alexandria, VA 22333-0001
1	Director U.S. Army Research Laboratory ATTN: AMSRL-OP-CI-AD, Tech Publishing 2800 Powder Mill Rd. Adelphi, MD 20783-1145
1	Director U.S. Army Research Laboratory ATTN: AMSRL-OP-CI-AD, Records Management 2800 Powder Mill Rd. Adelphi, MD 20783-1145
2	Commander U.S. Army Armament Research, Development, and Engineering Center ATTN: SMCAR-IMI-I Picatinny Arsenal, NJ 07806-5000
2	Commander U.S. Army Armament Research, Development, and Engineering Center ATTN: SMCAR-TDC Picatinny Arsenal, NJ 07806-5000
1	Director Benet Weapons Laboratory U.S. Army Armament Research, Development, and Engineering Center ATTN: SMCAR-CCB-TL Watervliet, NY 12189-4050
1	Director U.S. Army Advanced Systems Research and Analysis Office (ATCOM) ATTN: AMSAT-R-NR, M/S 219-1 Ames Research Center Moffett Field, CA 94035-1000

No. of Copies	Organization
1	Commander U.S. Army Missile Command ATTN: AMSMI-RD-CS-R (DOC) Redstone Arsenal, AL 35898-5010
1	Commander U.S. Army Tank-Automotive Command ATTN: AMSTA-JSK (Armor Eng. Br.) Warren, MI 48397-5000
1	Director U.S. Army TRADOC Analysis Command ATTN: ATRC-WSR White Sands Missile Range, NM 88002-5502
(Class. only) 1	Commandant U.S. Army Infantry School ATTN: ATSH-CD (Security Mgr.) Fort Benning, GA 31905-5660
(Unclass. only) 1	Commandant U.S. Army Infantry School ATTN: ATSH-WCB-O Fort Benning, GA 31905-5000
1	WL/MNOI Eglin AFB, FL 32542-5000
	Aberdeen Proving Ground
2	Dir, USAMSAA ATTN: AMXSY-D AMXSY-MP, H. Cohen
1	Cdr, USATECOM ATTN: AMSTE-TC
1	Dir, ERDEC ATTN: SCBRD-RT
1	Cdr, CBDA ATTN: AMSCB-CII
1	Dir, USARL ATTN: AMSRL-SL-I
10	Dir, USARL ATTN: AMSRL-OP-CI-B (Tech Lib)

No. of Copies	Organization
3	Commander U.S. Army Aviation Systems Command ATTN: AMSAV-ESC, G. Kovacs SFAE-AV-BH-T, R. Olson SFAE-AV-AAH-SA, D. Roby 4300 Goodfellow Blvd. St. Louis, MO 63120-1798
2	Commander AATD ATTN: AMSAT-R-TF, G. Hufstetler SAVRT-TY-ASV, H. Reddick USAATCOM Fort Eustis, VA 23604-5577
1	Commander ASC ATTN: ASC/XRM, G. Bennett AFSC Headquarters Wright-Patterson AFB, OH 45433-6503
1	Commander WRDC ATTN: WL/FIVST, M. Lentz AFSC Headquarters Wright-Patterson AFB, OH 45433-6553
1	Commander ATTN: ASC/XRYA, K. McArdle Eglin AFB, FL 32542
2	Commander Dahlgren Division Naval Surface Warfare Center ATTN: Code G-13, T. Wasmund D. Dickinson Dahlgren, VA 22448
1	McDonnell Douglas Helicopter Company ATTN: William Sims 5000 E. McDowell Rd. Mesa, AZ 85205
1	Boeing Helicopters Division ATTN: N. Caravasos P.O. Box 16858 Philadelphia, PA 19142

No. of Copies	Organization
1	Sikorsky Aircraft Mail Stop Z101A ATTN: G. Burblis 6900 Main St. Stratford, CT 06601-1381
	Aberdeen Proving Ground
1	Dir, USAMSAA ATTN: AMXSY-AD, C. Alston
43	Dir, USARL ATTN: AMSRL-SL-B (2 cps) (Bldg. 328) AMSRL-SL-BA (20 cps) (Bldg. 1065) AMSRL-SL-BA, K. Kim (20 cps) (Bldg. 1065) AMSRL-SL-N, M. Miller (Bldg. E3331)

USER EVALUATION SHEET/CHANGE OF ADDRESS

This Laboratory undertakes a continuing effort to improve the quality of the reports it publishes. Your comments/answers to the items/questions below will aid us in our efforts.

1. ARL Report Number ARL-TR-235 Date of Report October 1993

2. Date Report Received _____

3. Does this report satisfy a need? (Comment on purpose, related project, or other area of interest for which the report will be used.) _____

4. Specifically, how is the report being used? (Information source, design data, procedure, source of ideas, etc.) _____

5. Has the information in this report led to any quantitative savings as far as man-hours or dollars saved, operating costs avoided, or efficiencies achieved, etc? If so, please elaborate. _____

6. General Comments. What do you think should be changed to improve future reports? (Indicate changes to organization, technical content, format, etc.) _____

CURRENT ADDRESS

_____
Organization

_____
Name

_____
Street or P.O. Box No.

_____
City, State, Zip Code

7. If indicating a Change of Address or Address Correction, please provide the Current or Correct address above and the Old or Incorrect address below.

OLD ADDRESS

_____
Organization

_____
Name

_____
Street or P.O. Box No.

_____
City, State, Zip Code

(Remove this sheet, fold as indicated, tape closed, and mail.)
(DO NOT STAPLE)

DEPARTMENT OF THE ARMY

OFFICIAL BUSINESS

BUSINESS REPLY MAIL
FIRST CLASS PERMIT No 0001, APG, MD

Postage will be paid by addressee

Director
U.S. Army Research Laboratory
ATTN: AMSRL-OP-CI-B (Tech Lib)
Aberdeen Proving Ground, MD 21005-5066

NO POSTAGE
NECESSARY
IF MAILED
IN THE
UNITED STATES